Am J Nucl Med Mol Imaging 2015;5(1):27-37
www.ajnmmi.us /ISSN:2160-8407/ajnmmi0001546

Original Article

PET imaging of apoptosis in tumor-bearing mice and rabbits after paclitaxel treatment with ^{18}F-Labeled recombinant human His_{10}-annexin V

Haidong Qin[1], Ming-Rong Zhang[2], Lin Xie[2], Yanjie Hou[1], Zichun Hua[3], Minjin Hu[4], Zizheng Wang[1], Feng Wang[1,3]

[1]Nanjing First Hospital, Nanjing Medical University, 210006, China; [2]Department of Molecular Probes, Molecular Imaging Center, National Institute of Radiological Science, Chiba 263-8885, Japan; [3]State Key Laboratory of Pharmaceutical Biotechnology, Department of Biochemistry, Nanjing University, Nanjing 210093, China; [4]Changzhou High-Tech Research Institute of Nanjing University and Jiangsu Target Pharma Laboratories Inc, Changzhou 213164, China

Received July 25, 2014; Accepted September 2, 2014; Epub December 15, 2014; Published January 1, 2015

Abstract: Monitoring response to chemo- or radiotherapy is of great importance in clinical practice. Apoptosis imaging serves as a very useful tool for the early evaluation of tumor response. The goal of this study was PET imaging of apoptosis with ^{18}F-labeled recombinant human annexin V linked with 10 histidine tag (^{18}F-rh-His_{10}-annexin V) in nude mice bearing an A549 tumor and rabbits bearing a VX2 lung cancer after paclitaxel therapy. ^{18}F-rh-His_{10}-annexin V was prepared by conjugation of rh-His_{10}-annexin V with *N*-succinimidyl 4-[^{18}F]fluorobenzoate. Biodistribution was determined in mice by the dissection method and small-animal PET. Single-dose paclitaxel (175 mg/m^2) was used to induce apoptosis in A549 and VX2 tumor models. ^{18}F-rh-His_{10}-annexin V was injected into A549 mice and VX rabbits to acquire dynamic and static PET images 72 h after paclitaxel treatment. The uptake of ^{18}F-rh-His_{10}-annexin V in apoptotic cells 4 h after induction was 6.45±0.52 fold higher than that in non-induced cells. High focal uptake of ^{18}F-rh-His_{10}-annexin V was visualized in A549 (SUV_{max}: 0.35±0.13) and VX2 (0.41±0.23) tumor models after paclitaxel treatment, whereas lower uptake was found in the corresponding tumors before treatment (A549 SUV_{max}: 0.04±0.02; VX2: 0.009±0.002). The apoptotic index was 75.61±11.56% in the treated VX2 cancer, much higher than that in the untreated VX2 (8.03±2.81%). This study demonstrated the feasibility of ^{18}F-rh-His_{10}-annexin V for the detection of apoptosis after chemotherapy in A549 and VX2 tumor models.

Keywords: Apoptosis, molecular imaging, recombinant human His_{10}-annexin V, tumor response

Introduction

Detection of the early responses of tumors to treatment is critical for guiding subsequent therapy, allowing rapid selection of the most appropriate therapy. Tumor response to treatment is conventionally assessed by measuring tumor size with anatomical imaging such as CT or MRI [1]. However, there are several fundamental and practical limitations using purely anatomic measurements as a survival proxy. Tumor shrinkage can take weeks or even months to become apparent or, with some therapies, might not occur at all, despite a positive response to treatment [2]. ^{18}F-FDG PET is well established in the clinical diagnosis, staging and management of malignant tumors [3, 4], and has been used for early evaluation of tumor therapy response in many varieties of malignant tumor [5-9]. Persistently focal uptake of FDG after therapy always indicates a poor response and prognosis. However, FDG uptake is influenced by various factors, including blood glucose level, tumor sizes, inflammation, and acquisition protocol. Furthermore, slowly-growing, metabolically less active tumors including thyroid and prostate cancer and neuroendocrine tumor are not sensitive to FDG PET.

Apoptosis is the most common pathway for therapy-induced cancer cell elimination and lack of apoptosis is usually a sign of therapy failure [10, 11]. Non-invasive molecular imaging of apoptosis is of considerable interest for

assessing the therapy outcome and evaluating disease progression [12, 13]. In the past decade, annexin V binding has become the main measurement of apoptosis in histopathology. To detect apoptosis after chemo- or radiotherapy, in vivo imaging with ^{99m}Tc-labeled annexin V and analogs has been performed and is well documented [14-24]. Our prior study showed that apoptosis imaging can monitor the response of non-small cell lung tumor graft to paclitaxel therapy. A positive correlation was shown between the uptake of radioactivity and TUNEL staining in the tumor areas [25]. Our latest study showed that ^{99m}Tc-rh-His$_{10}$-annexin V can detect apoptosis in a porcine model with ischemia and reperfusion [26]. However, most of the ^{99m}Tc-labeled annexin V tracers displayed high uptake in the liver and kidney, which hampers the clinical application [27, 28].

Because PET has higher resolution and is more quantitative than SPECT imaging with a ^{99m}Tc-labeled tracer, ^{18}F-labeled annexin V has been developed and used for imaging apoptosis by many research groups. ^{18}F-annexin V showed lower uptake in the liver and abdomen than ^{99m}Tc-annexin V, and could detect apoptosis in myocardial reperfusion injury and in the liver with cycloheximide treatment [29-32].

The current study aims to evaluate ^{18}F-rh-His$_{10}$-annexin V as a PET tracer for detecting apoptosis and early assessment of the outcome of paclitaxel chemotherapy in A549 tumor-bearing mouse and VX2 lung cancer-bearing rabbit models. In this study, we used recombinant human annexin V linked with a ten histidine tag (rh-His$_{10}$-annexin V) at the *N* terminal of annexin V. This histidine tag simplified the purification of annexin V protein by ion exchange chromatography. The present study describes data about ^{18}F-rh-His$_{10}$-annexin V for the detection of apoptosis from a nude mice graft tumor model to rabbit VX2 tumor.

Materials and methods

General

^{18}F was produced by the ^{18}O (p, n) ^{18}F nuclear reaction using a CYPRIS HM-18 cyclotron (Sumitomo Heavy Industry, Tokyo). If not otherwise stated, radioactivity was determined with an IGC-3R Curiemeter (Aloka, Tokyo). HPLC was performed using a JASCO HPLC system (JASCO, Tokyo): effluent radioactivity was monitored using a NaI (Tl) scintillation detector system. If not indicated, all chemical reagents of the highest grade commercially available were purchased from Sigma-Aldrich (St. Louis, MO) and Wako Pure Chem. Ind. (Osaka, Japan).

Expression and purification of rh-His$_{10}$-annexin V

Human annexin V cDNA was cloned into plasmid pET19b and fused to a ten consecutive histidine tag at N-terminal [33]. By ammonium sulfate precipitation and two types of ion exchange chromatography, rh-His$_{10}$-annexin V was purified to homogeneity with purity over 97%.

Synthesis of ^{18}F-rh-His$_{10}$-annexin V

[^{18}F]F$^-$ was produced by the ^{18}O (p, n) ^{18}F reaction on 95 atom % $H_2{}^{18}O$ from the cyclotron. [^{18}F]F$^-$ in aqueous K_2CO_3 (3.3 mg/0.3 mL) was transported into a vial containing CH_3CN (1.5 mL)/Kryptofix 222 (15 mg) in a hot cell and was dried at 110°C for 15 min. To the dried [^{18}F]F$^-$ was added a solution of 10 mg ethyl 4-(trimethylammonium triflate) benzoate in 0.2 mL anhydrous DMSO. This reaction mixture was heated at 110°C for 15 min. Hydrolysis of benzoate was performed by heating the mixture with 0.5 mL 1 N NaOH at 95°C for 10 min. After the mixture had been cooled for 2 min, 0.8 mL 1 N HCl was added. The reaction mixture was diluted to final volume of 15 mL with distilled water and loaded onto a Waters Sep-Pak cartridge that was activated in advance using 30 mL CH_3CN and 30 mL distilled water. The loaded cartridge was washed with 2 mL 0.01 N HCl and dried for 2 min with a nitrogen stream. The radioactive fraction containing 4-^{18}F-fluorobenzoic acid was eluted with 1.5 mL CH_3CN.

The above radioactive fraction was heated with 20 μL 10% aqueous $(CH_3)_4NOH$ solution for 15 min. After CH_3CN had been removed with a nitrogen stream at 90°C, 1.5 mL anhydrous CH_3CN was added and removed again. A solution of *O*-(*N*-succinimidyl)-*N,N,N',N'*-tetramethyluronium tetrafluoroborate (15 mg) in 1 mL CH_3CN was added and the reaction mixture was heated at 90°C for 5 min. This mixture was concentrated to 0.2 mL, cooled down, and diluted with 0.2 mL 5% aqueous acetic acid. HPLC semi-preparative purification of the mix-

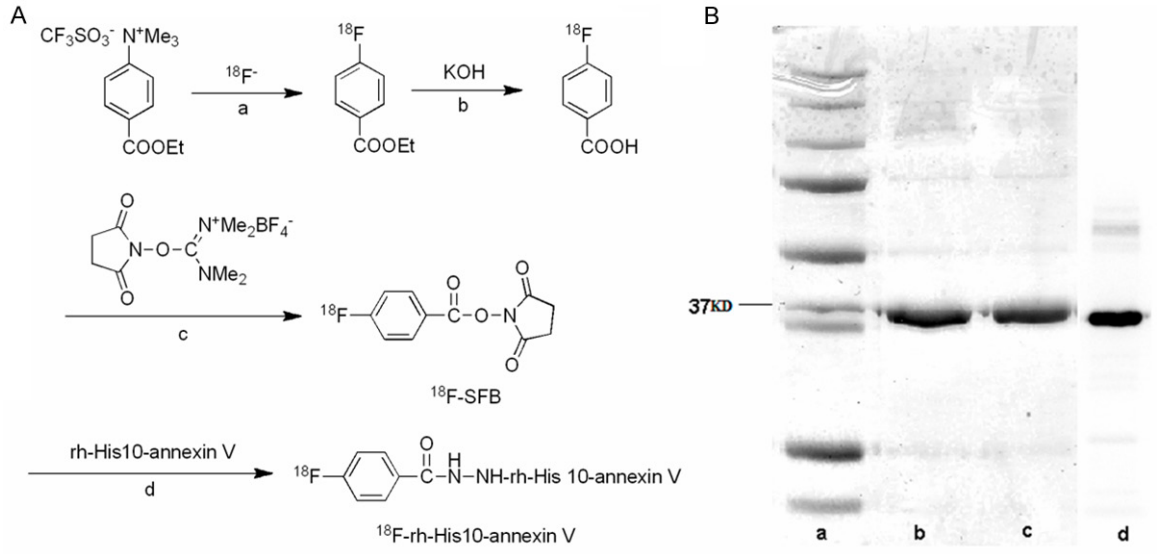

Figure 1. A: Synthesis scheme of ^{18}F-rh-His$_{10}$-annexin V. Reaction conditions include a: 110°C, CH_3CN, 15 min; b: 95°C, 10 min; c: $(CH_3)_4NOH$, 90°C, CH_3CN, 5 min; d: 0.1 M borate buffer, room temperature, 20 min. B: Lane a, marker. Lane b, Wild type annexin V. Lane c, Recombinant His$_{10}$-annexin V. Lane d. Autoradiography.

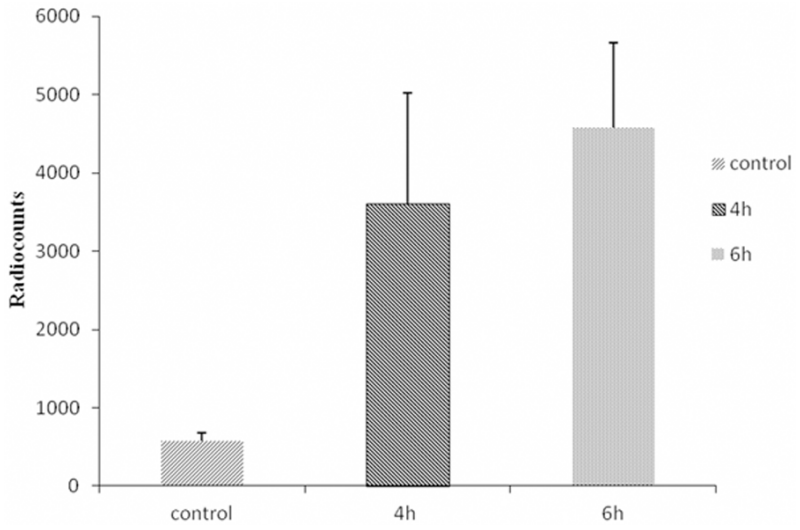

Figure 2. *In vitro* binding assay indicated that ^{18}F-rh-His$_{10}$-annexin V could bind to apoptotic cells specifically. Radiouptake in paclitaxel treatment cells was significantly higher than that in control, at 4 h, 6 h after treatment.

ture was performed on a YMC J'sphere ODS-H80 column (10 mm internal diameter ×250 mm) using a mobile phase of CH_3CN/H_2O (60/40) at 4.0 mL/min. The fraction of *N*-succinimidyl 4-^{18}F-fluorobenzoate (^{18}F-SFB, retention time: 10.5 min) was collected, diluted with 10 mL distilled water, and loaded to a Waters Sep-Pak cartridge. This cartridge was dried with a nitrogen stream and eluted with 2.5 mL CH_3CN. The CH_3CN eluent containing ^{18}F-SFB was collected and evaporated to dryness under a gentle nitrogen stream at room temperature. The synthesis scheme was shown in (**Figure 1A**)

A solution of ^{18}F-SFB in 0.2 M borate buffer pH 8.4 (50 μL) was added to a solution of rh-His$_{10}$-annexin V (200 μg) in borate buffer pH 8.4 (50 μL). The mixture was kept at room temperature for 20 min. The reaction mixture was purified with size-exclusion column chromatography using Bio-Gel P-6 (BIO-RAD) according to the standard procedure.

Radiochemical purity determination

Radiochemical purity was assayed by analytical HPLC (Bio-Rad HPLC Gel Filtration, Bio-Sil EC-125, 7.8 mm 300 mm; 0.05 M NaH_2PO_4/0.05 M Na_2HPO_4/0.2 M NaCl: 1/1/1). The retention time for ^{18}F-rh-His$_{10}$-annexin V was 6.3 min at 1.0 mL/min.

SDS PAGE

SDS-PAGE was performed with a Mini-PROTEIN and POWER PAC 300 (Bio-Rad, Hercules, CA).

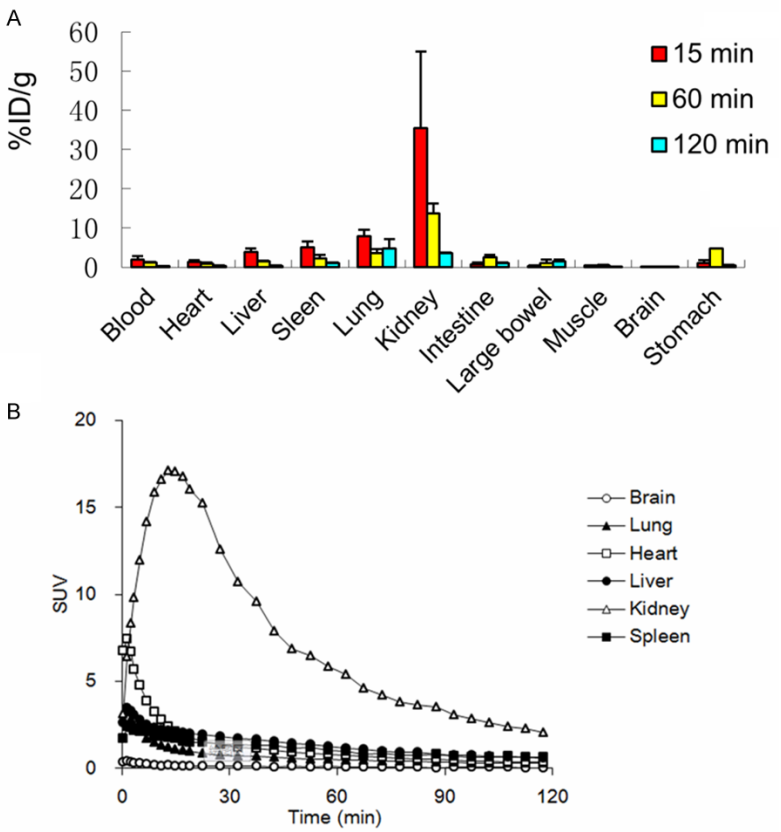

Figure 3. A: Biodistribution of ^{18}F-rh-His$_{10}$-annexin V in mice at 15 min, 1 h and 2 h after injection (n=3). The radioactivity was expressed as ID %/g. B: Time-radioactivity curves in main organs were acquired with small-animal PET, the radioactivity was expressed as SUV.

Laemmli sample buffer (Bio-Rad) was added to each sample (1/1) and applied to Ready-gels J (Bio-Rad). Precision Protein Standard (Bio-Rad) was used as a standard. Electrophoresis was performed under constant voltage (200 V). After electrophoresis, gels were exposed to an imaging plate and radioactivity was analyzed by an imaging system (BAS5000, Fuji Photo Film, Tokyo, Japan), followed by staining with Bio-Safe Coomassie.

In vitro binding assays

Apoptosis was induced in Jurkat cells (RIKEN Cell Bank, Wako, Japan) at a density of 5×10^6 cells/mL using 3.5 μmol/L camptothecin (Sigma-Aldrich) for 4 h and 6 h. About 74 KBq of ^{18}F-rh-His$_{10}$-annexin V was incubated with 500 μL apoptotic or untreated cells (5×10^5) in 15 mM *N*-(2-hydroxythyl)piperazine-*N*-9-(2-ethanesulfonic acid), 120 mM NaCl and 2 mM $CaCl_2$, pH 7.4, respectively. To separate binding cells from free ^{18}F-rh-His$_{10}$-annexin V, the mixture was centrifuged at 1,000 g for 2 min. After removing the aqueous supernatant, the left radioactivity was measured with a 1480 Wizard gamma counter (Perkin-Elmer, Walthan, MA).

Biodistribution study in mice

Male ddY mice (20~30 g, 7 weeks old; SLC, Shizuoka, Japan) were used. Each mouse was injected with ^{18}F-rh-His$_{10}$-annexin V (0.37 MBq/200 μL) via the tail vein. Three mice were sacrificed by cervical dislocation at 15 min, 60 min and 120 min after injection. Whole brain, liver, heart, lung, stomach, kidney, spleen, intestine and blood sample were removed quickly. Radioactivity was measured using a 1480 Wizard autogamma scintillation counter (Perkin-Elmer) and expressed as a percent of the injected dose per gram tissue (% ID/g) with the mean±standard deviations. All radioactivity was corrected for decay.

Metabolite analysis

After intravenous injection of ^{18}F-rh-His$_{10}$-annexin V (2.14 MBq/200 μL) in ddY mice, these mice were sacrificed by cervical dislocation at 120 min. Blood samples were acquired immediately and centrifuged at 15000 rpm for 1 min at 4°C, which of 250 μL plasma was acquired after centrifuge. At the same time point, 100 μL urine was collected. Fifty microliter of plasma and urine were analyzed by HPLC with the same parameters for the determination of radiochemical purity. The ratio of ^{18}F-rh-His$_{10}$-annexin V o total radioactivity on the HPLC chromatogram was analyzed and calculated as a percentage.

In vivo imaging with small-animal PET

PET scan was performed using a small-animal PET Inveon scanner (Siemens Medical Solutions

Table 1. Biodistribution of ^{18}F-rh-His$_{10}$-annexin V in mice at 15 min, 1 h, 2 h after injection

Organs	15 min	60 min	120 min
Blood	2.00±0.85	1.12±0.25	0.28±0.04
Heart	1.31±0.45	0.91±0.26	0.37±0.03
Liver	3.89±0.90	1.48±0.18	0.36±0.07
Spleen	5.03±1.55	2.24±1.54	1.09±0.07
Lung	7.89±1.70	1.54±1.04	0.81±0.31
Kidney	35.43±19.46	13.75±2.41	3.56±0.22
Intestine	0.81±0.33	2.52±0.60	0.98±0.18
Large bowel	0.34±0.15	1.05±0.85	1.56±0.39
Muscle	0.39±0.13	0.51±0.08	0.17±0.03
Brain	0.09±0.04	0.05±0.01	0.02±0.01
Stomach	1.08±0.77	4.70±3.55	0.42±0.14

The radioactivity was expressed as ID %/g (n=3).

USA). Prior to the scans, a mouse was anesthetized with 1.5% (v/v) isoflurane and positioned on the scanner bed. After transmission scans for attenuation correction were performed for 2 cycles (803 sec) using a ^{57}Co point source, dynamic emission scans were acquired for 120 min in a 3D list mode with an energy window of 350~650 keV, immediately after intravenous injection of 1.85 MBq [^{18}F]rh-His$_{10}$-annexin V. All list-mode data were sorted into 3D sinograms, which were then Fourier rebinned into 2D sinograms (frames: 4×1, 8×2 and 20×5 min). Dynamic images were reconstructed with filtered back-projection using a Ramp filter. For data analysis, region of interest (ROI) were drawn on lung, heart, liver, and kidney using ASIPro VM (Analysis Tools and System Setup/Diagnostics Tool), the time-radioactivity curve, Standard uptake value (SUV) and ID%/g were acquired automatically. SUV_{max} was calculated by measuring the maximal concentration of radioactivity in a ROI and correcting it for body weight and injected dose (SUV_{max}=maximum activity concentration/[injected dose/body weight]) in A549 tumor model.

Preparation of A549 nude mice tumor model and VX2 rabbit lung tumor model

A549 tumor cells were cultured as a monolayer in Dulbecco's modified Eagle's F-12 medium supplemented with 10% fetal bovine serum. Female nude mice (BALB/c) weighing 18~22 g were inoculated subcutaneously in the anterior chest wall with an average 5×10^6 A549 tumor cells per site. When the tumor size reached 0.5-1.0 cm in diameter, which required about 2 weeks, the mice were separated into 2 groups (5 mice per each group). One group received paclitaxel (175 mg/m^2) by injection into the tail vein, another without treatment served as control.

Eight New Zealand white rabbits (Nanjing Medical University) weighing 2~3 kg were used. VX2 tumor is the biggest tumor model, which closely resembles human cancer. VX2 cells were initially grown in the hind limb of a donor rabbit. Each rabbit received general anesthesia with 3% pentobarbital (30 mg/kg) through an indwelling catheter in the auricular vein. VX2 tumor was surgically removed from a donor rabbit under general anesthesia and minced into 1-mm^3 pieces with a pair of scissors. After receiving anesthesia, two 1.0-cm-deep tunnels were made bilaterally into the skin of the front chest, and one or two 1-mm^3 pieces of VX2 tissue were implanted into each tunnel. The incisions were closed with 3.0 sutures. When the tumors had grown to approximately 1~2 cm in diameter, the rabbit was used in the experiment. Six VX2 tumor rabbits received a single dose of paclitaxel (175 mg/m^2), two served as control.

Image interpretation in A549 tumor model

After ^{18}F-rh-His$_{10}$-annexin V (3.7 MBq) injected via the tail vein, a dynamic scan was performed for 120 min after injection and static images were acquired from 105 min to 120 min. PET scans were performed in mice with A549 before and after paclitaxel treatment. For data analysis, ROIs were drawn on the tumor and peripheral organs using ASIPro VM.

After imaging, the mice were scarified. In the A549 tumor model, hematoxylin and eo-sin (H&E) staining was performed to verify apoptosis occurrence in the frozen sections. DNA fragmentation was analyzed by terminal deoxynucleotidytransferase mediated-dUTP nick-end labeling (TUNEL) assay using an ApopTag peroxidase in situ oligonucleotide (oligo) ligation (ISOL) apoptosis detection kit (S7200; Chemicon/Millipore, Billerica, MA) according to the manufacturer's protocol.

Imaging and interpretation in VX2 tumor model

Six rabbits bearing a VX2 tumor were treated by intravenous injection of paclitaxel at a dose of

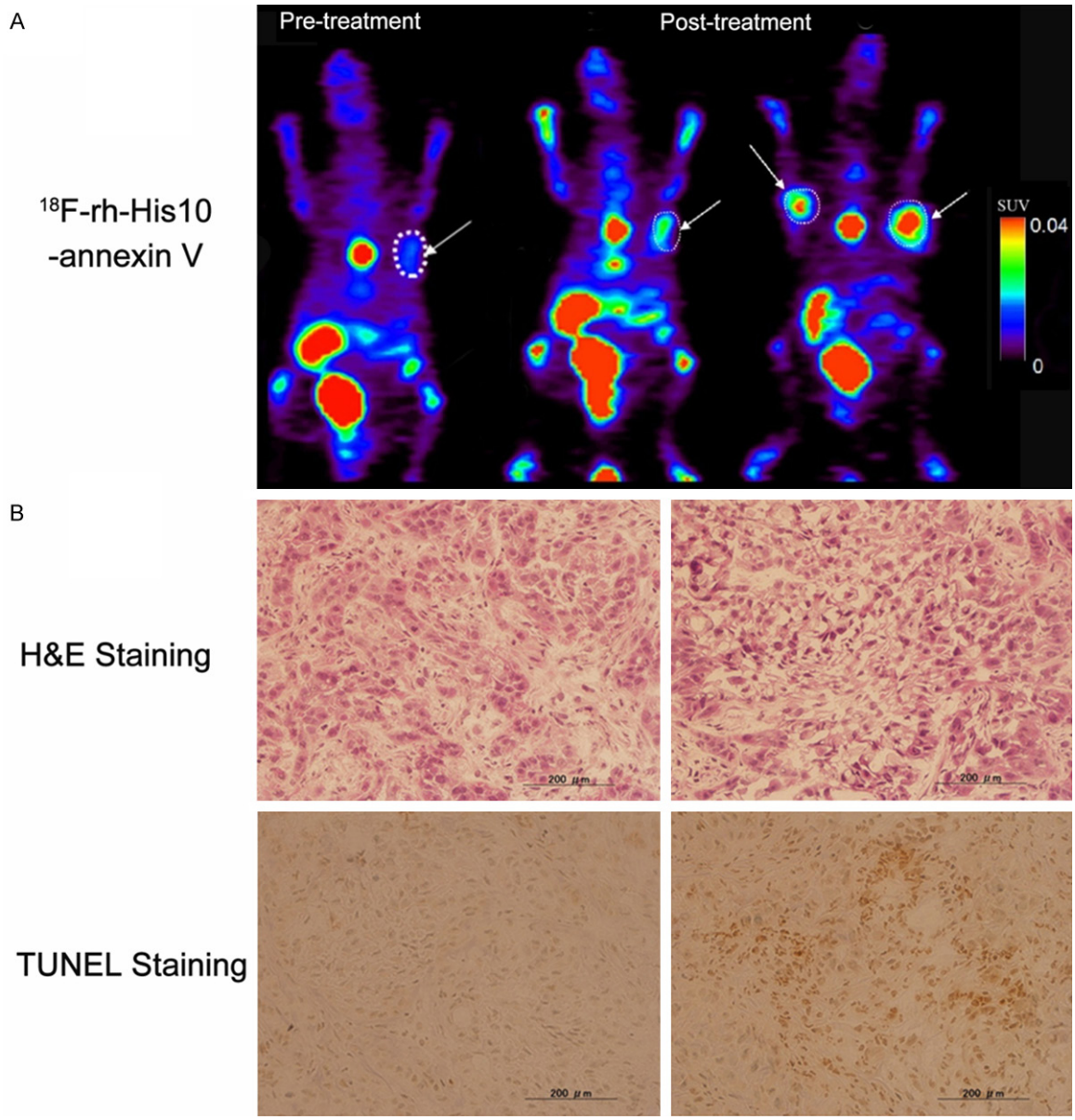

Figure 4. Representative PET images of ^{18}F-rh-His$_{10}$-annexin V in A549 tumor model (A). Left: Image in the tumor before treatment, Middle and Right: after paclitaxel treatment (Middle, same xenegraft with before treatment, Right, another mouse xenograft). Histological staining (B): Much more apoptotic cells were presented in the tumor after treatment in comparison of baseline image. The tumor was indicated by white arrow.

175 mg/m^2. Before and 72 h after treatment, ^{18}F-rh-His$_{10}$-annexin V (18.5~37 MBq) was injected via the auricular vein, PET-CT (Philips Medical System) was performed 60 min after injection. Two of the VX2 tumor model rabbits served as a control and did not receive treatment. PET scans with ^{18}F-FDG (37 MBq) were performed using the same rabbits. Each PET/CT scan was performed 60 min after injection. Emission data were acquired at 3 min per bed position and CT component was performed using a multi-detector scanner before the emission component. The parameters included 140 kV, 80 mA, 0.8 s per CT rotation, a pitch of 5.0 mm, and a table speed of 22.5 mm/s. Images were analyzed visually and quantified with SUV_{max} based on attenuation-corrected images.

After imaging, the rabbits were sacrificed and formalin-fixed paraffin-embedded tumor tissues were excised after imaging. DNA fragmen-

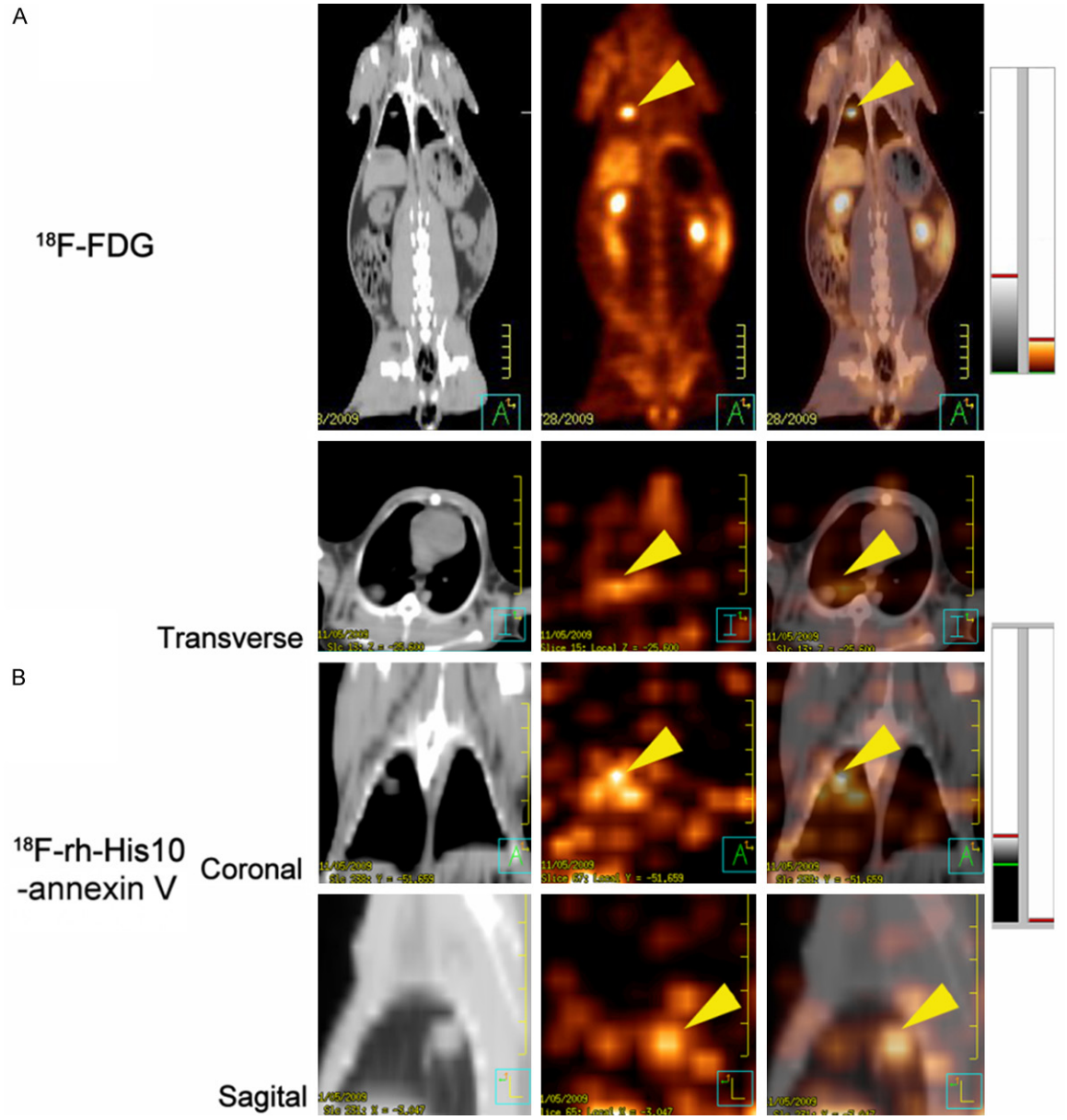

Figure 5. A: ^{18}F-FDG image: Focal uptake was showed in the VX2 lung cancer before treatment. B: ^{18}F-rh-His$_{10}$-annexin V in transverse, coronal and sagittal image showed intense uptake in the tumor 72 h after treatment. The tumor was indicated by yellow arrow head.

tation were analyzed by TUNEL assay using a commercial kit (Maxin-Bio) according the manufacturer's protocol. In random fields, TUNEL-positive nuclei as a percentage of total nuclei was determined and used as the apoptotic index.

Statistical analysis

All data are expressed as the mean±SD, statistical analysis was performed using SPSS 10.0, t tests were used to compare the treated group and untreated controls, $p < 0.05$ was considered significant.

Results

Synthesis of ^{18}F-rh-His$_{10}$-annexin V

The decay corrected radiochemical yield of ^{18}F-rh-His$_{10}$-annexin V was 20~25% based on ^{18}F-SFB with a synthesis time of 90 min from the end of bombardment. At the end of synthesis, 130~160 MBq of ^{18}F-rh-His$_{10}$-annexin V was obtained as an *i.v.* injectable solution with

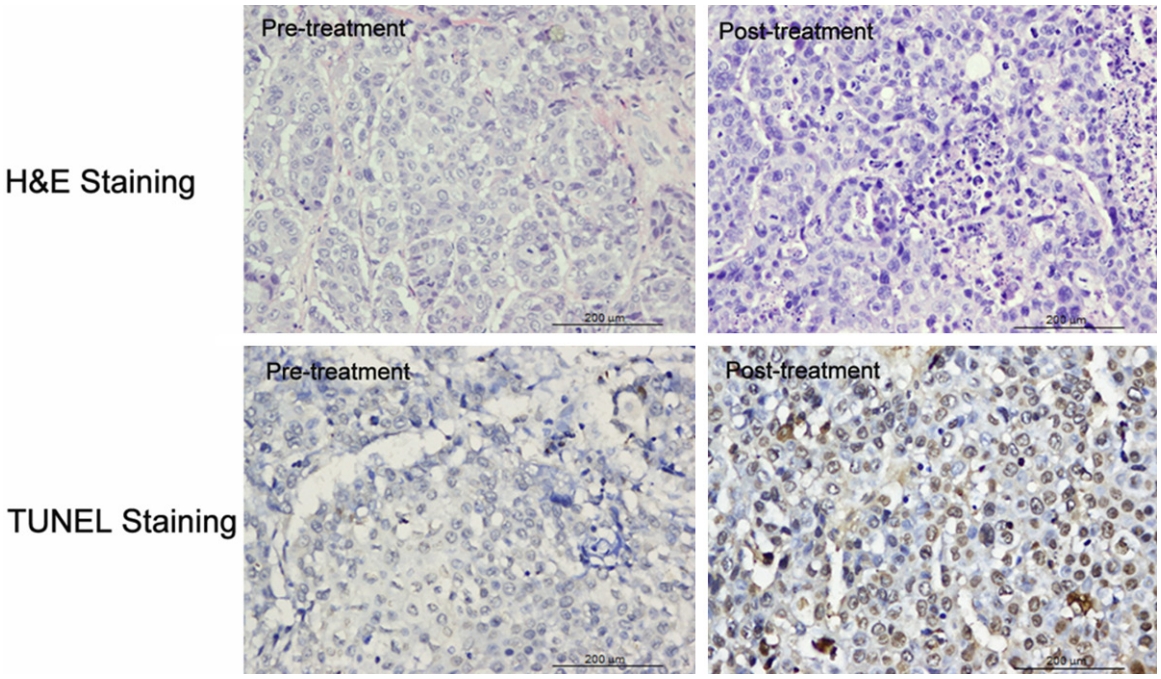

Figure 6. Histological staining in VX2 Lung cancer showed a small number of apoptotic cells were found before treatment, whereas a large number of apoptotic cells were observed after the treatment. TUNEL-positive nuclei confirmed the DNA fragmentation.

a radiochemical purity of > 98% determined by HPLC. The autoradiograph and Coomassie staining of polyacrylamide after electrophoresis further verified the radiochemically pure product (**Figure 1B**), no degradation was observed during radiolabeling and synthesis.

In vitro binding assay

The binding specificity of ^{18}F-rh-His$_{10}$-annexin V was evaluated with camptothecin-induced Jurkat cells. After inducement, apoptotic cells was observed at 4 h and 6 h. Incubation with ^{18}F-rh-His$_{10}$-annexin V showed that the uptake of radioactivity in the induced cells was 6.45±0.52 fold and 8.12±0.45 fold higher than that of the untreated cells ($p < 0.01$), respectively (**Figure 2**).

Biodistribution on mice

The biodistrbution profile of ^{18}F-rh-His$_{10}$-annexin V uptake in normal mice was shown in (**Figure 3A**, **Table 1**). The most predominant uptake was shown in the kidney, and the radioactivity decreased rapidly to less than 10% of the maximum level 120 min after injection. At 15 min after injection, lower uptake was found in non-specific peripheral organs, such as the heart, gastrointestinal tract and skeletal muscles. Rapid clearance of radioactivity was observed in blood, the uptake value was 0.28±0.04 ID%/g at 120 min after injection.

Time-radioactivity curves in the main organs are shown in (**Figure 3B**). The initial high uptake was visualized in the liver and heart, which represented the uptake of blood pool. The liver uptake peaked at 1.5 min after injection, decreased rapidly to a low level. The kidney uptake reached the maximum at 20 min and then decreased until the end of PET scan.

Metabolite analysis

Metabolite analysis of ^{18}F-rh-His$_{10}$-annexin V was performed for mouse plasma and urine. At 120 min after injection, about 60% of total radioactivity represented the unchanged ^{18}F-rh-His$_{10}$-annexin V in the plasma. On the other hand, 74% of total radioactivity in the urine represented the radiolabeled metabolites at 120 min.

PET imaging for mice and histopathology

High focal uptake of ^{18}F-rh-His$_{10}$-annexin V was visualized in the A549 tumor after treatment by

paclitaxel (**Figure 4A**, the Middle and Right image), whereas lower uptake was seen A549 mice before treatment (**Figure 4A**, Left image). The SUV_{max} in tumor after treatment was 0.35±0.13, significantly higher than the group before treatment (0.04±0.02, *P < 0.001*). After paclitaxel treatment, a large number of apoptotic cells were observed. H&E and TUNEL staining showed that the apoptotic cells increased in the treated group compared to the untreated group (**Figure 4B**).

PET imaging for rabbits and histopathology

Representative images of VX2 rabbit lung cancer were shown in (**Figure 5**) ^{18}F-FDG image showed high focal uptake in the primary tumor before treatment (**Figure 5A**), whereas no significant uptake of ^{18}F-rh-His$_{10}$-annexin V was found in FDG avid foci. After paclitaxel treatment, ^{18}F-rh-His$_{10}$-annexin V images showed intense uptake in the tumor (**Figure 5B**). By analyzing the images of treatment and the untreated controls, the SUV_{max} of ^{18}F-rh-His$_{10}$-annexin V after treatment was 0.41±0.23, that of the untreated group was 0.009±0.002 (*t=0.78, P < 0.001*).

Histological analysis showed a small number of apoptotic cells were found before treatment, which were characterized by cell shrinkage, condensed nuclei, and the appearance of apoptotic bodies, after the treatment, a large number of apoptotic cells were observed (**Figure 6**). TUNEL-positive nuclei confirmed the DNA fragmentation. The apoptotic index was 75.61±11.56% in the treated group, significantly higher than that in the control (8.03±2.81%; *P < 0.001*).

Discussion

^{18}F-rh-His$_{10}$-annexin V was prepared by labeling rh-His$_{10}$-annexin V with ^{18}F-SFB. Radiolabeling was reproducible with 20~35% radiochemical yield based on ^{18}F-SFB. After size-column exclusion chromatography, the radiochemical purity of this ^{18}F-labeled radiotracer exceeded 95%. Further, the radiochemical purity remained > 90% after standing the product at 25°C for 3 h. No degradation of protein was found during the synthesis and maintaining processes. This result indicates radiochemical stability of ^{18}F-rh-His$_{10}$-annexin V within the time of at least one PET scan. The analytical results were in compliance with our in-house quality control/assurance specifications of radiopharmaceuticals.

^{18}F-rh-His$_{10}$-annexin V can bind to apoptotic Jurkat cells induced by camptothecin, and the uptake in the induced cells was higher than that of untreated cells. Despite the introduction of a ten histidine tag, the specific binding of this protein to apoptotic cells was not affected. The in vitro results confirmed that ^{18}F-rh-His$_{10}$-annexin V was worth in vivo evaluation and had shown its usefulness.

^{18}F-rh-His$_{10}$-annexin V showed a superior biodistribution profile compared with ^{99m}Tc-labeled-annexin V [27-28]. PET dynamic data further confirmed that it mainly excreted from kidney and urinary system, rapid clearance from blood and liver was observed. This finding indicates that the ^{18}F-labeled tracer may have more benefits for the detection of apoptosis than ^{99m}Tc-labeled-annexin V, which usually showed slow excretory clearance and relatively high uptake in the liver and spleen. On the other hand, metabolite analysis showed a high percentage of radiolabeled metabolite in the mouse urine at 120 min after injection of ^{18}F-rh-His$_{10}$-annexin V, which may contribute to the lower uptake of radioactivity in the kidney.

In nude mice bearing A549 tumor, focal uptake was visualized in the tumor after paclitaxel treatment. VX2 is the biggest tumor model and closely imitate human lung cancer initiation, development and progress. In VX2 lung cancer, as shown in **Figure 5**, multiple FDG avid foci was found before treatment, while high uptake of ^{18}F-rh-His$_{10}$-annexin V was shown in the tumor 72 h after treatment, the SUVmax in the tumor after therapy was much higher than in the untreated group. A large number of TUNEL-positive nuclei were observed after treatment. H&E staining also revealed the presence of a large number of apoptotic cells associated with cell shrinkage, condensed nuclei and apoptotic bodies. Only a small number of apoptotic cells were confirmed in the control. This finding revealed that increased accumulation of ^{18}F-rh-His$_{10}$-annexin V in the tumor after paclitaxel treatment was caused by ongoing apoptosis. The present PET study with ^{18}F-rh-His$_{10}$-annexin V showed that this radiotracer is feasible to

detect apoptosis after chemotherapy not only in A549 nude mice tumor model but in VX2 lung cancer as a mimic of human lung cancer.

Conclusions

This study demonstrated the feasibility of ^{18}F-rh-His$_{10}$-annexin V for the detection of apoptosis after chemotherapy from A549 graft to VX2 lung tumor models which could imitate the development and progress of human cancer. The current study will serve as a reference point that gauges the early tumor therapy outcome with apoptosis imaging.

Acknowledgements

We thank the staff of the National Institute of Radiological Sciences for support in the cyclotron operation, radioisotope production, and animal experiments. This research was supported by the Jiangsu Provincial Nature Science Foundation (BL2012037, BK2011104, BK20-06010), the Chinese National Nature Sciences Foundation (81271604, 81171383).

Disclosure of conflict of interest

The authors have no conflict of interest.

Address correspondence to: Dr. Zizheng Wang or Dr. Feng Wang, Department of Nuclear Medicine, Nanjing First Hospital, Nanjing Medical University, Nanjing 210006, China. E-mail: zzwang@aliyun.com (ZZW); fengwangcn@hotmail.com (FW)

References

[1] Michaelis LC and Ratain MJ. Measuring response in a post-RECIST world: from black and white to shades of grey. Nat Rev Cancer 2006; 6: 409-14.

[2] Goffin J, Baral S, Tu D, Nomikos D and Seymour L. Objective responses in patients with malignant melanoma or renal cell cancer in early clinical studies do not predict regulatory approval. Clin Cancer Res 2005; 11: 5928-34.

[3] Weber WA. Positron emission tomography as an imaging biomarker. J Clin Oncol 2006; 24: 3282-92.

[4] Gambhir SS. Molecular imaging of cancer with positron emission tomography. Nat Rev Cancer 2002; 2: 683-93.

[5] Juweid ME and Cheson BD. Positron-emission tomography and assessment of cancer therapy. N Engl J Med 2006; 354: 496-507.

[6] Avril N, Sassen S, Schmalfeldt B, Naehrig J, Rutke S, Weber WA, Werner M, Graeff H, Schwaiger M, Kuhn W. Prediction of response to neoadjuvant chemotherapy by sequential F-18-fluorodeoxyglucose positron emission tomography in patients with advanced-stage ovarian cancer. J Clin Oncol 2005; 23: 7445-53.

[7] Hicks RJ. Role of 18F-FDG PET in assessment of response in non-small cell lung cancer. J Nucl Med 2009; 50 Suppl 1: 31S-42S.

[8] Weber WA and Wieder H. Monitoring chemotherapy and radiotherapy of solid tumors. Eur J Nucl Med Mol Imaging 2006; 33 Suppl 1: 27-37.

[9] Cheson BD, Pfistner B, Juweid ME, Gascoyne RD, Specht L, Horning SJ, Coiffier B, Fisher RI, Hagenbeek A, Zucca E, Rosen ST, Stroobants S, Lister TA, Hoppe RT, Dreyling M, Tobinai K, Vose JM, Connors JM, Federico M, Diehl V; International Harmonization Project on Lymphoma. Revised response criteria for malignant lymphoma. J Clin Oncol 2007; 25: 579-86.

[10] Blankenberg FG. In vivo detection of apoptosis. J Nucl Med 2008; 49 Suppl 2: 81S-95S.

[11] Kim R. Recent advances in understanding the cell death pathways activated by anticancer therapy. Cancer 2005; 103: 1551-60.

[12] Brindle K. New approaches for imaging tumour responses to treatment. Nat Rev Cancer 2008; 8: 94-107.

[13] Fulda S and Debatin KM. Extrinsic versus intrinsic apoptosis pathways in anticancer chemotherapy. Oncogene 2006; 25: 4798-811.

[14] Michalski MH and Chen X. Molecular imaging in cancer treatment. Eur J Nucl Med Mol Imaging 2010; 38: 358-77.

[15] Russo A, Terrasi M, Agnese V, Santini D and Bazan V. Apoptosis: a relevant tool for anticancer therapy. Ann Oncol 2006; 17 Suppl 7: vii115-23.

[16] Hersey P, Zhang XD and Mhaidat N. Overcoming resistance to apoptosis in cancer therapy. Adv Exp Med Biol 2008; 615: 105-26.

[17] Blankenberg FG, Katsikis PD, Tait JF, Davis RE, Naumovski L, Ohtsuki K, Kopiwoda S, Abrams MJ, Darkes M, Robbins RC, Maecker HT, Strauss HW. In vivo detection and imaging of phosphatidylserine expression during programmed cell death. Proc Natl Acad Sci U S A 1998; 95: 6349-54.

[18] Dumont EA, Reutelingsperger CP, Smits JF, Daemen MJ, Doevendans PA, Wellens HJ, Hofstra L. Real-time imaging of apoptotic cell-membrane changes at the single-cell level in the beating murine heart. Nat Med 2001; 7: 1352-5.

[19] Petrovsky A, Schellenberger E, Josephson L, Weissleder R and Bogdanov A Jr. Near-infrared

fluorescent imaging of tumor apoptosis. Cancer Res 2003; 63: 1936-42.
[20] Hofstra L, Liem IH, Dumont EA, Boersma HH, van Heerde WL, Doevendans PA, De Muinck E, Wellens HJ, Kemerink GJ, Reutelingsperger CP, Heidendal GA. Visualization of cell death in vivo in patients with acute myocardial infarction. Lancet 2000; 356: 209-12.
[21] Belhocine T, Steinmetz N, Li C, Green A and Blankenberg FG. The imaging of apoptosis with the radiolabeled annexin V: optimal timing for clinical feasibility. Technol Cancer Res Treat 2004; 3: 23-32.
[22] Kartachova M, van Zandwijk N, Burgers S, van Tinteren H, Verheij M and Valdes Olmos RA. Prognostic significance of 99mTc Hynic-rh-annexin V scintigraphy during platinum-based chemotherapy in advanced lung cancer. J Clin Oncol 2007; 25: 2534-9.
[23] Kartachova MS, Valdes Olmos RA, Haas RL, Hoebers FJ, van Herk M and Verheij M. 99mTc-HYNIC-rh-annexin-V scintigraphy: visual and quantitative evaluation of early treatment-induced apoptosis to predict treatment outcome. Nucl Med Commun 2008; 29: 39-44.
[24] van de Wiele C, Lahorte C, Vermeersch H, Loose D, Mervillie K, Steinmetz ND, Vanderheyden JL, Cuvelier CA, Slegers G, Dierck RA. Quantitative tumor apoptosis imaging using technetium-99m-HYNIC annexin V single photon emission computed tomography. J Clin Oncol 2003; 21: 3483-7.
[25] Wang F, Fang W, Zhao M, Wang Z, Ji S, Li Y, Zheng Y. Imaging paclitaxel (chemotherapy)-induced tumor apoptosis with 99mTc C2A, a domain of synaptotagmin I: a preliminary study. Nucl Med Biol 2008; 35: 359-64.
[26] Ye F, Fang W, Wang F, Hua ZC, Wang Z and Yang X. Evaluation of adenosine preconditioning with 99mTc-His10-annexin V in a porcine model of myocardium ischemia and reperfusion injury: preliminary study. Nucl Med Biol 2011; 38: 567-74.
[27] Rottey S, Slegers G, Van Belle S, Goethals I, Van de Wiele C. Sequential 99mTc-hydrazinonicotinamide-annexin V imaging for predicting response to chemotherapy. J Nucl Med 2006; 47: 1813-8.
[28] Lahorte CM, Vanderheyden JL, Steinmetz N, Van de Wiele C, Dierckx RA, Slegers G. Apoptosis-detecting radioligands: current state of the art and future perspectives. Eur J Nucl Med Mol Imaging 2004; 31: 887-919.
[29] Tait JF, Smith C and Blankenberg FG. Structural requirements for in vivo detection of cell death with 99mTc-annexin V. J Nucl Med 2005; 46: 807-15.
[30] Zijlstra S, Gunawan J and Burchert W. Synthesis and evaluation of a 18F-labelled recombinant annexin-V derivative, for identification and quantification of apoptotic cells with PET. Appl Radiat Isot 2003; 58: 201-7.
[31] Murakami Y, Takamatsu H, Taki J, Tatsumi M, Noda A, Ichise R, Tait JF, Nishimura S. 18F-labelled annexin V: a PET tracer for apoptosis imaging. Eur J Nucl Med Mol Imaging 2004; 31: 469-74.
[32] Yagle KJ, Eary JF, Tait JF, Grierson JR, Link JM, Lewellen B, Gibson DF, Krohn KA. Evaluation of 18F-annexin V as a PET imaging agent in an animal model of apoptosis. J Nucl Med 2005; 46: 658-66.
[33] Zhang LN, Yang X and Hua ZC. Expression and purification of recombinant human annexin V in Escherichia coli. Prep Biochem Biotechnol 2000; 30: 305-12.